JOURNAL OF GEOPHYSICAL RESEARCH, VOL. 111, D21206, doi:10.1029/2006JD007150, 2006

Cosmic ray induced ionization in the atmosphere: Full modeling and practical applications

Ilya G. Usoskin[1] and Gennady A. Kovaltsov[2]

Received 2 February 2006; revised 12 April 2006; accepted 7 August 2006; published 8 November 2006.

[1] We present a physical model to calculate cosmic ray induced ionization in the atmosphere. The model is based on the Monte Carlo CORSIKA tool, which simulates full development of an electromagnetic-muon-nucleonic cascade in the atmosphere, with the FLUKA package used for low-energy interactions. The direct ionization by primary cosmic rays is explicitly taken into account. The model is applicable to the entire atmosphere, from the ground up to the stratosphere. A comparison to fragmentary direct measurements of the ionization in the atmosphere confirms the validity of the model in the whole range of geographical latitudes and altitudes. Results of the full Monte Carlo simulation are tabulated in a form of the ionization yield function. These tables are given together with a detailed recipe, which allows a user to compute easily the cosmic ray induced ionization for given location, altitude and the spectrum of cosmic rays. This provides a new tool for a quantitative study of the space weather influence upon the Earth's environment. Some practical applications are discussed.

Citation: Usoskin, I. G., and G. A. Kovaltsov (2006), Cosmic ray induced ionization in the atmosphere: Full modeling and practical applications, *J. Geophys. Res.*, *111*, D21206, doi:10.1029/2006JD007150.

1. Introduction

[2] Presently, there are numerous arguments suggesting that the solar magnetic variability affects the global climate in different aspects and on different timescales [see, e.g., *Gleisner and Thejll*, 2003; *Haigh et al.*, 2005; *Shaviv*, 2005]. The existing evidence, however, is based mostly on empirical correlations, while the nature of this connection still needs to be understood in terms of quantitative mechanism, responsible for the observed correlations. Several possible mechanisms have been suggested, which can be responsible for the observed relation between the solar variability and the climate: via the changing solar irradiance [*Fröhlich and Lean*, 2004; *Soon*, 2005]; by the UV heating of the stratosphere and consequent changes in the circulation patterns [*Haigh*, 1994, 1996]; or by cosmic rays affecting the cloud formation [*Tinsley*, 1996; *Marsh and Svensmark*, 2003]. However, they are qualitative schemes where some quantitative links are still missing. In particular, the latter mechanism is related to the cosmic ray induced ionization (CRII) of the atmosphere as first proposed by *Ney* [1959]. Energetic cosmic rays (CR) initiate a nucleonic-electromagnetic cascade in the atmosphere, affecting its physical-chemical properties, in particular the ion balance [see *Dorman*, 2004, and references therein]. This is a dominant source of ionization of the troposphere. Therefore a detailed model of the CRII makes a solid basis for a quantitative study of the mechanism presumably affecting cloud formation. On the other hand, CRII is a key factor affecting the atmospheric chemistry [e.g., *Vitt and Jackman*, 1996]. Until recently it was commonly considered that the CRII is proportional to the cosmic ray flux, as measured by ground based neutron monitors [e.g., *Marsh and Svensmark*, 2003]. However, that is not fully correct [*Dorman and Dorman*, 2005; *Aplin et al.*, 2005], and explicit computations of the CRII are required for a detailed quantitative study [e.g., *Pallé et al.*, 2004; *Usoskin et al.*, 2004b].

[3] Two approaches have been developed to compute the CRII. One model (see the full description in [*O'Brien*, 2005]) is based on an analytical approximation of the atmospheric cascade, while the other is based on a Monte Carlo simulation of the atmospheric cascade [*Usoskin et al.*, 2004a; *Desorgher et al.*, 2005]. Using the latter method, we have recently built a basic CRII model which, however, has some shortcomings: it is static, it neglects the direct ionization by primaries in the stratosphere and it is valid only for the troposphere. Here we present an improved Monte Carlo model, whose validity range has been extended to cover the atmosphere up to the stratospheric altitudes. The new model is based on an updated version of the CORSIKA code, including the FLUKA Monte Carlo package to simulate the low-energy nuclear interactions, and explicitly the direct ionization by primary CR particles. We present here the details of the model (section 2) and provide a detailed recipe as well as the tabulated ionization yield function (section 2.5), which allows a user to compute the CRII easily. Possible applications of the model are discussed in section 3.

2. Model Calculations

2.1. Technical Details

[4] The present model is based on the full Monte Carlo simulation of the electromagnetic-muon-nucleonic cascade, initiated by primary cosmic rays in the Earth's atmosphere.

[1]Oulu Unit, Sodankylä Geophysical Observatory, University of Oulu, Oulu, Finland.
[2]Ioffe Physical-Technical Institute, St. Petersburg, Russia.

0148-0227/06/2006JD007150$09.00

The Monte Carlo simulations have been performed using the CORSIKA (Cosmic Ray Simulations for Kascade) simulation tool [*Heck et al.*, 1998], using its updated version (v. 6.204, July 2005, see the full description at http://www-ik.fzk.de/corsika). The EGS4 model [*Nelson et al.*, 1985], which explicitly simulates all the interactions of electrons, positrons and photons in the atmosphere, has been used for simulating the electromagnetic interactions. High-energy hadronic interactions have been simulated using the HDPM set of routines [*Capdevielle et al.*, 1992]. Interactions of low-energy (below 80 GeV of total energy) hadrons were treated with the FLUKA (v.2003b) tool [*Fassò et al.*, 2001]. Our previous model [*Usoskin et al.*, 2004a] treated low-energy hadronic interactions using the GHEISHA2002 routine, which has been shown to have deficiencies in the simulated kinematics of low-energy interactions [*Heck et al.*, 2003]. Note that most of the secondary particles, ionizing the ambient air, are treated by a low-energy model even if the energy of primaries was high. Therefore an update of the low-energy interaction model from GHEISHA to FLUKA is crucial for the improved CRII calculations.

[5] We used a realistic curved atmosphere to allow computing CRII at high altitudes. The chemical composition of the atmosphere was taken as N_2, O_2 and Ar in the volume fractions of 78.1%, 21% and 0.9%, respectively. The atmosphere's density profile was modeled by five regions. Within each region, the density profile was individually approximated by an exponential law, according to the standard U.S. atmosphere parameterized by *Keilhauer et al.* [2004, see Table 13]. Since the muon's life time is close to the time of its flight in the atmosphere, the results depend on exact atmospheric density profile. In order to minimize this uncertainty, we computed the CRII per gram of the atmospheric matter rather than per cm^3. In this case, the uncertainties of the CRII, computed using different atmospheric density profiles, do not exceed 1–2% in the low troposphere and are below 1% for higher altitudes, which is less than statistical errors of computations.

2.2. Ionization Yield Function

[6] First we have computed the ionization yield function Y which gives the number of ion pairs produced in one gram of the ambient air at a given atmospheric depth by one nucleon of the primary cosmic ray particle with the given energy per nucleon. (Throughout the paper we will consider kinetic energy per nucleon.) For each value of the primary particle's energy we have performed a set of many cascade simulations. In each individual simulation within the set, the primary cosmic ray particles with the fixed energy have been simulated to impinge isotropically onto the curved atmosphere, with the zenith angle between 0 and 90°. The results of all the simulation runs have been averaged within the set. The number of the simulated cascades depends on the energy of the primaries, and varies between 10,000,000 cascades for low-energy particles and 1,000 cascades for the highest energies. The lowest and the highest of the computed kinetic energies were 0.07 GeV/nuc and 1000 GeV/nuc, respectively, with 5 energy values per one order of magnitude (1, 2, 3, 5 and 7) thus leading to 22 energy channels.

[7] The atmosphere has been divided in computational layers of thickness $\Delta x = 10$ g/cm^2. In each layer, the energy deposited because of ionization losses has been computed separately for three principal components: electromagnetic (e^-, e^+ and photons), hadron and muon. Because of an intrinsic limitation of the CORSICA model, the kinetic energy of all hadrons below 50 MeV was considered to be transformed into ionization losses in the local layer.

[8] The ionization yield function Y (ion pairs sr cm^2 g^{-1}), which corresponds to the atmospheric depth x, the primary cosmic rays with the kinetic energy T and the unit unidirectional flux (particles sr^{-1} cm^{-2}), is:

$$Y(x,T) = \pi \frac{\Delta E}{E_i \Delta x} \tag{1}$$

where ΔE is the mean energy losses in the atmospheric layer centered at the atmospheric depth x per one simulated primary nucleon with the kinetic energy T, and $E_i = 35$ eV is the average energy needed to produce one ion pair [*Porter et al.*, 1976], and $\pi = 2\pi \int \cos\theta \sin\theta d\theta$ is the geometrical normalizing factor (θ being the zenith angle varying between 0 and 90°).

[9] Figure 1 shows samples of the total ionization yield function together with the contributions from the three principal components of the cascade: electromagnetic, muon and hadronic. Contributions of these components vary at different altitudes in the atmosphere. For low-energy primaries, the entire ionization is defined solely by the hadronic component (Figure 1a). On the contrary, ionization induced by high-energy cosmic rays (Figure 1c) is dominated by the secondary muons in the lower troposphere ($x < 600$ g/cm^2) and by the electromagnetic component at higher altitudes. The contribution from the hadronic component is negligible in this case. For middle energies all the three components are equally important, but each dominates at certain altitudes: the electromagnetic component at high altitudes ($x < 300$ g/cm^2), the muon component near the ground ($x > 900$ g/cm^2), and the hadronic component dominates in between. Therefore all the three components are important, but play their roles at different altitudes and different energy ranges of primary particles. The total ionization yield function for the primary protons is shown in Figure 2a for different atmospheric depths. The ionization rate decreases with the atmospheric depth and increases with the energy of primary particles. The yield function is very steep in the lower-energy part, where it is dominated by the hadronic component, and becomes flatter with increasing energy, where the muon component takes over. Note that, while an α-particle is nearly identical to four protons in the high energy range in the sense of CRII (grey curve in Figure 2a), it produces more ion pairs in the lower energy range. Hence it is important to consider α-particles separately. In the sense of produced ionization, heavier nuclei can be considered as nearly identical to the corresponding number of α-particles, e.g., a ^{56}Fe nucleus can be substituted by 14 α-particles. We have verified the validity of this approach for ^{14}N and ^{56}Fe nuclei by direct Monte Carlo simulations.

[10] In Tables 1 and 2 we give a reduced tabulated version of the ionization yield function for the protons and α-particles, respectively, while the full version (with a detailed resolution in the energy and the atmospheric depth)

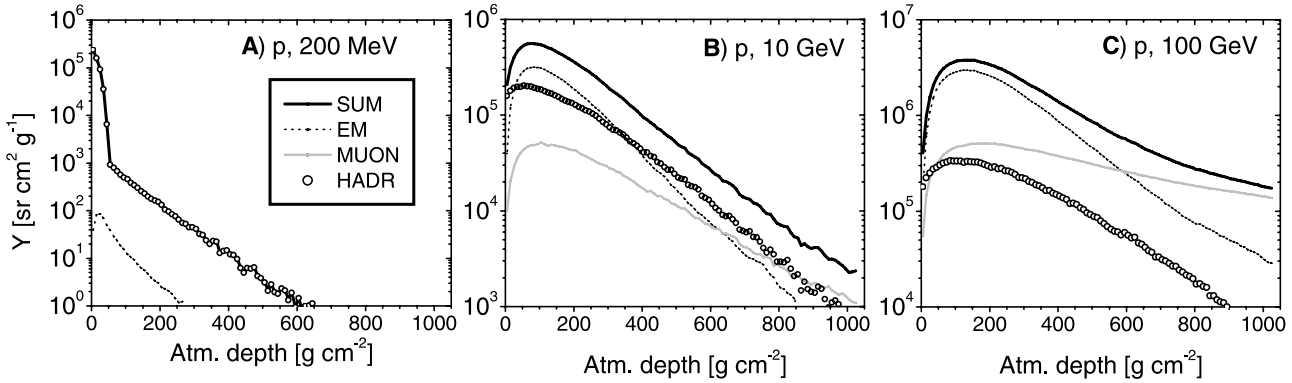

Figure 1. Ionization yield function Y according to the Monte Carlo simulations of the atmospheric cascade for primary protons with energy (a) 0.2 GeV, (b) 10 GeV and (c) 100 GeV isotropically impinging on the Earth's atmosphere. Curves represent ionization by the electromagnetic (dotted), the muon (grey) and the hadronic components (open dots) of the cascade, as well as the total ionization (solid curve). Note different vertical axis scales.

is given in the supplement materials. A recipe of computing the CRII using these tables is discussed in section 2.5.

2.3. Cosmic Ray Spectrum

[11] It is common for various applications to parameterize the differential energy spectrum of galactic cosmic rays at the Earth's orbit by the so-called force field model [*Gleeson and Axford*, 1968; *Caballero-Lopez and Moraal*, 2004; *McCracken et al.*, 2004a], where the spectrum of ith specie (with the charge number Z_i and the mass number A_i) of CR at Earth's orbit, J_i, is related to an unmodulated local interstellar spectrum (LIS) of the same specie, $J_{\mathrm{LIS},i}$ via the modulation potential ϕ (given in MV) as:

$$J_i(T,\phi) = J_{\mathrm{LIS},i}(T+\Phi_i)\frac{(T)(T+2T_\mathrm{r})}{(T+\Phi_i)(T+\Phi_i+2T_\mathrm{r})}, \qquad (2)$$

where T is the particle's kinetic energy (in MeV/nuc), $\Phi_i = (eZ_i/A_i)\phi$, and T_r = 938 MeV/nuc is the proton's rest mass. The modulation potential provides a good single-parameter approximation of the actual shape of the CR spectrum near Earth [*Usoskin et al.*, 2005]. An implicit parameter of the force field approximation is the shape of the LIS, which is not well known. Here we use the LIS for protons according to [*Burger et al.*, 2000]

$$J_{\mathrm{LIS},p}(T) = \frac{1.9\cdot P(T)^{-2.78}}{1+0.4866\,P(T)^{-2.51}}, \qquad (3)$$

where $P(T) = \sqrt{T(T+2T_r)}$. J and T are expressed in the units of nucleons/(cm^2 sr s GeV/nuc) and GeV/nuc, respectively, and T_r = 0.938 Gev/nuc. This equation corresponds to equation (2) of *Burger et al.* [2000] within 2% accuracy, but it is easier to use and corrects a typographical error in the latter (ln P should be read instead of P on the second line there (R. A. Burger and M. S. Potgieter, personal communication, 2002)).

[12] The complex nuclei, in particular α-particles, are approximately twice as rigid as the hydrogen nuclei with the same energy per nucleon, hence the fraction of the heavier species in the overall CR flux near Earth is increasing with decreasing particle's energy and increasing modulation potential [see, e.g., *Usoskin et al.*, 2005]. Some calculated spectra of cosmic protons and α-particles are shown in Figure 2b for typical solar maximum (ϕ = 1000 MV) and minimum (ϕ = 400 MV) modulation conditions. The LIS of the heavier species has been taken of the same shape as the LIS of protons (equation (2)) but scaled to match the abundance ratios in the interstellar space [*Alcaraz et al.*, 2000; *Usoskin et al.*, 2005]. Since the heavier species are identical to α-particles, both in the heliospheric modulation ($Z/A \approx 1/2$) and in the induced ionization, we consider all the nuclei, heavier than protons, as α-particles with the corresponding number of nucleons. The nucleonic ratio of heavier nuclei (including α-particles) to protons is chosen to be 0.3 in the interstellar space [e.g., *Gaisser and Stanev*, 2004], i.e., (compare equation (3)):

$$J_{\mathrm{LIS},\alpha}(T) = \frac{0.57\cdot P(T)^{-2.78}}{1+0.4866\,P(T)^{-2.51}}, \qquad (4)$$

2.4. Cosmic Ray Induced Ionization

[13] By multiplying of the ionization yield function (Figure 2a) by the CR spectrum (Figure 2b), one obtains the differential ionization function for the ith specie of CR:

$$F_i(x,T,\phi) = Y_i(x,T)\cdot J_i(T,\phi). \qquad (5)$$

An example of the ionization function F_p for protons is shown in Figure 2c, where ϕ = 700 MV (the mean modulation potential for the last solar cycles), and several values of the atmospheric depth are considered. One can see that the most effective energy of cosmic rays for ionization depends on the atmospheric depth. The maximum ionization in the stratosphere is produced by particles with an energy of about 1 GeV/nuc. The peak, corresponding to the most effective energy, moves toward higher energies with decreasing altitude, being about 3 GeV/nuc at x = 700 g/cm^2. At the sea level, the differential ionization function has a flat top in the energy range 3–30 GeV/nuc. The summary

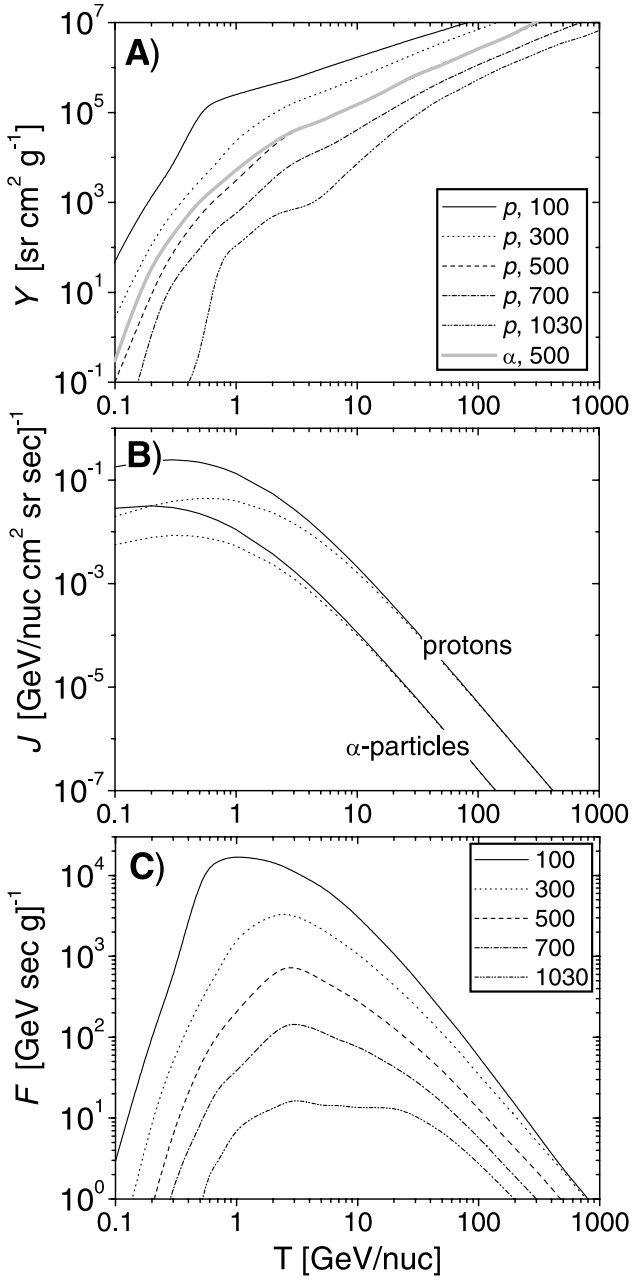

Figure 2. (a) Ionization yield function for primary cosmic rays. Different curves correspond to different atmospheric depths as denoted in the legend in units of g/cm^2. Black curves, denoted by p, correspond to primary protons, while the grey curve, denoted by α, corresponds to primary α-particles. (b) Differential energy spectra of primary galactic protons (top curves) and α-particles (bottom curves) near Earth for the solar activity minimum ($\phi = 400$ MV, solid curves) and maximum ($\phi = 1000$ MV, dotted curves) conditions. (c) Differential ionization function F for primary protons at different atmospheric depths as denoted in the legend in units of g/cm^2. The proton spectrum corresponds to $\phi = 700$ MV.

ionization rate in the atmosphere can be presented as a sum of the ionization rates Q_i due to different species of GCR:

$$Q(x,\phi) = \sum_i Q_i = \sum_i \int_{T_{c,i}}^{\infty} J_i(T,\phi)\ Y_i(x,T)\ dT, \qquad (6)$$

where Y_i is the ionization yield function and J_i is the differential energy spectrum of the ith specie of GCR. The ionization rate Q is given in the units of ion pairs g^{-1} s^{-1}. Integration is over the kinetic energy above $T_{c,i}$, which is the kinetic energy corresponding to the local geomagnetic rigidity cutoff P_c. This cutoff energy (per nucleon) depends on the Z/A ratio of the cosmic ray specie and is given as

$$T_{c,i} = \sqrt{\left(\frac{Z_i}{A_i}\right)^2 P_c^2 + T_r^2} - T_r, \qquad (7)$$

where $T_r = 0.938$ GeV/nuc is the proton's rest mass. This implies that particles with the ratio of $Z/A < 1$ are less deflected by the geomagnetic field, which, in combination with their weaker heliospheric modulation, makes them very important in the CRII. While a precise determination of P_c requires complex computations of the test particles' trajectories in a realistic magnetic field configuration [*Smart et al.*, 2000], it can be approximately computed using the Störmer's approximation [*Elsasser et al.*, 1956]:

$$P_c \approx 1.9 \cdot M \cos^4 \lambda_G, \qquad (8)$$

where P_c is the vertical geomagnetic cutoff yielded in GV, M is the dipole moment of the geomagnetic field expressed in 10^{22} Am^2, and λ_G is the local geomagnetic latitude. The present value of $M = 7.8\ 10^{22}$ Am^2 corresponds to $P_c \approx 14.8$ GV at the magnetic equator. Note that the geomagnetic field slowly changes in time, varying in both the dipole moment M and the geomagnetic pole migration (leading to the varying λ_G for a given geographical location). All these changes affect CRII on long timescales and should be properly taken into account (see section 3). Equation (8) does not account for realistic directional geomagnetic cutoffs but it provides a reasonable first-order approximation [e.g., *Cooke*, 1983; *O'Brien*, 2005] to the effective cutoff for isotropically impinging flux. Although this approach is supported by the agreement between our results and the measurements, it may be a source of uncertainties, and detailed computations of cosmic ray transport in the magnetosphere are needed.

2.5. Numerical Recipe

[14] By means of the above formalism, one can easily compute the CRII for a given altitude x, location P_c and time (or actually, the modulation potential ϕ), using the following recipe.

[15] 1. Tabulated values of the ionization yield function $Y(x, T)$ are given in Tables 1 and 2 (or, in more details, in the electronic supplementary materials) for protons and α-particles.

[16] 2. The value of the modulation potential ϕ can be obtained for a given period from *Usoskin et al.* [2005] or from http://cosmicrays.oulu.fi/phi. The shape of the differential energy spectrum $J(T, \phi)$ is then calculated using equations (2)–(4) for both species.

Table 1. Ionization Yield Function $Y_p(x, T)$ (Ion Pairs sr cm^2 g^{-1}) for Primary Cosmic Protons With the Given Kinetic Energy Given in GeV/nuc (Columns 3–11)[a]

x	ρ	0.1	0.3	1	3	10	30	100	300	1000
25	3.8E-5	3.4E+2	4.1E+5	4.6E+5	6.0E+5	1.3E+6	2.3E+6	4.9E+6	8.5E+6	1.5E+7
75	1.2E-4	9.8E+1	4.3E+4	3.3E+5	6.3E+5	1.8E+6	4.2E+6	1.0E+7	2.3E+7	5.7E+7
125	2.0E-4	5.0E+1	4.4E+3	2.1E+5	5.2E+5	1.6E+6	4.4E+6	1.2E+7	2.9E+7	8.3E+7
175	2.7E-4	2.0E+1	2.5E+3	1.3E+5	4.0E+5	1.3E+6	3.8E+6	1.1E+7	3.0E+7	9.3E+7
225	3.5E-4	7.9E+0	1.4E+3	7.4E+4	2.9E+5	9.9E+5	3.1E+6	9.9E+6	2.8E+7	9.2E+7
275	4.2E-4	4.9E+0	8.5E+2	4.1E+4	2.1E+5	7.3E+5	2.4E+6	8.1E+6	2.4E+7	8.2E+7
325	4.8E-4	2.0E+0	4.9E+2	2.1E+4	1.5E+5	5.3E+5	1.8E+6	6.3E+6	2.0E+7	6.9E+7
375	5.4E-4	8.1E-1	2.9E+2	1.1E+4	1.0E+5	3.7E+5	1.4E+6	5.0E+6	1.6E+7	5.7E+7
425	5.9E-4	3.1E-1	1.8E+2	6.2E+3	7.2E+4	2.6E+5	1.0E+6	3.9E+6	1.3E+7	4.5E+7
475	6.5E-4	0	1.1E+2	3.9E+3	5.0E+4	1.9E+5	7.4E+5	3.1E+6	1.1E+7	3.7E+7
525	7.1E-4	0	6.3E+1	2.6E+3	3.5E+4	1.4E+5	5.6E+5	2.4E+6	8.5E+6	2.9E+7
575	7.6E-4	0	3.8E+1	1.5E+3	2.4E+4	9.8E+4	4.4E+5	1.9E+6	6.9E+6	2.4E+7
625	8.2E-4	0	1.8E+1	1.1E+3	1.6E+4	7.2E+4	3.5E+5	1.6E+6	5.7E+6	2.0E+7
675	8.7E-4	0	1.3E+1	7.3E+2	1.0E+4	5.3E+4	2.7E+5	1.3E+6	4.7E+6	1.7E+7
725	9.2E-4	0	6.3E+0	4.2E+2	6.9E+3	3.8E+4	2.2E+5	1.1E+6	3.9E+6	1.4E+7
775	9.7E-4	0	5.0E+0	3.1E+2	5.1E+3	2.9E+4	1.8E+5	9.3E+5	3.4E+6	1.2E+7
825	1.0E-3	0	4.9E+0	1.8E+2	3.0E+3	2.1E+4	1.5E+5	8.3E+5	3.0E+6	1.0E+7
875	1.1E-3	0	1.2E+0	1.1E+2	1.7E+3	1.4E+4	1.3E+5	7.3E+5	2.6E+6	9.1E+6
925	1.1E-3	0	2.3E+0	9.9E+1	1.7E+3	1.2E+4	1.1E+5	6.6E+5	2.4E+6	8.1E+6
975	1.2E-3	0	8.9E-1	6.0E+1	8.0E+2	9.0E+3	9.6E+4	6.0E+5	2.2E+6	7.3E+6
1025	1.2E-3	0	1.8E-1	6.8E+1	7.0E+2	7.4E+3	8.5E+4	5.5E+5	2.0E+6	6.7E+6

[a]Columns 1 and 2 depict the atmospheric depth x (g cm^{-2}), and the corresponding density ρ (g cm^{-3}), respectively.

[17] The final CRII is computed using equation (6), where the integration bounds are different for the two species of GCR (see equation (7)).

2.6. Test of the Model

[18] We have verified our calculations of the CRII by confronting them with real measurements of the ionization rate in the atmosphere. There have been numerous balloon-borne measurements of the CRII performed at different conditions, and we have selected those covering the entire possible range of the conditions. Figure 3 shows a comparison of our model calculations (curves) to the measurements (symbols) for three different conditions: in the polar atmosphere during the solar maximum (Figure 3a); in the polar atmosphere during the solar minimum, i.e., the highest modern ionization rate (Figure 3b); and at the equator during the solar maximum, i.e., the lowest modern ionization rate (Figure 3c). One can see a good agreement between the model and the measurements below $\approx$17 km ($x > 100$ g/cm^2) for all conditions. Equally good agreement is obtained also for midlatitude observations (not shown). We note that individual measurements, performed during short balloon flights, can vary depending, e.g., on the exact atmospheric profile, the instrumentation, etc. [*Lowder et al.*, 1972]. On the other hand, the model CRII was computed for average conditions (the standard atmospheric profile, average modulation potential). Therefore we do not expect to precisely reproduce observations, and the agreement within 10% is considered as good. In the upper part of the atmosphere (above 18 km, $x < 100$ g/cm^2), the model yields

Table 2. Ionization Yield Function $Y_\alpha(x, T)$ (Ion Pairs sr cm^2 g^{-1}) for Primary α-Particles With the Given Kinetic Energy in GeV/nuc (Columns 3–11)[a]

x	ρ	0.1	0.3	1	3	10	30	100	300	1000
25	3.8E-5	1.0E+3	3.7E+5	4.1E+5	5.8E+5	1.3E+6	2.5E+6	5.5E+6	8.6E+6	2.2E+7
75	1.2E-4	3.4E+2	3.5E+4	3.0E+5	6.2E+5	1.9E+6	4.6E+6	1.2E+7	2.7E+7	6.8E+7
125	2.0E-4	1.6E+2	9.9E+3	1.9E+5	5.3E+5	1.8E+6	4.8E+6	1.4E+7	3.5E+7	9.6E+7
175	2.7E-4	6.5E+1	5.6E+3	1.3E+5	4.1E+5	1.4E+6	4.2E+6	1.3E+7	3.7E+7	1.1E+8
225	3.5E-4	2.8E+1	3.4E+3	7.8E+4	3.1E+5	1.1E+6	3.4E+6	1.1E+7	3.5E+7	1.0E+8
275	4.2E-4	2.4E+1	2.0E+3	4.7E+4	2.2E+5	7.5E+5	2.6E+6	8.9E+6	3.1E+7	9.7E+7
325	4.8E-4	1.4E+1	1.2E+3	2.8E+4	1.6E+5	5.5E+5	2.0E+6	6.9E+6	2.6E+7	8.3E+7
375	5.4E-4	2.9E+0	7.5E+2	1.7E+4	1.1E+5	3.9E+5	1.5E+6	5.3E+6	2.0E+7	6.8E+7
425	5.9E-4	1.9E+0	4.6E+2	1.2E+4	8.0E+4	2.8E+5	1.1E+6	4.1E+6	1.6E+7	5.4E+7
475	6.5E-4	1.1E+0	2.8E+2	7.8E+3	5.3E+4	2.0E+5	8.5E+5	3.1E+6	1.2E+7	4.2E+7
525	7.1E-4	5.7E-1	1.8E+2	5.0E+3	3.7E+4	1.4E+5	6.4E+5	2.5E+6	9.9E+6	3.3E+7
575	7.6E-4	2.3E-1	1.0E+2	2.8E+3	2.4E+4	1.0E+5	4.8E+5	2.0E+6	8.0E+6	2.6E+7
625	8.2E-4	9.2E-3	7.7E+1	2.1E+3	1.8E+4	7.9E+4	3.8E+5	1.6E+6	6.5E+6	2.1E+7
675	8.7E-4	0	3.7E+1	1.5E+3	1.2E+4	5.0E+4	2.8E+5	1.4E+6	5.4E+6	1.7E+7
725	9.2E-4	0	2.0E+1	6.6E+2	7.4E+3	3.6E+4	2.3E+5	1.1E+6	4.6E+6	1.4E+7
775	9.7E-4	0	1.6E+1	6.3E+2	5.5E+3	3.0E+4	1.8E+5	9.7E+5	4.0E+6	1.2E+7
825	1.0E-3	0	8.2E+0	4.4E+2	4.1E+3	1.9E+4	1.5E+5	8.6E+5	3.4E+6	1.0E+7
875	1.1E-3	0	9.0E+0	2.5E+2	2.4E+3	1.4E+4	1.3E+5	7.5E+5	3.0E+6	8.8E+6
925	1.1E-3	0	6.7E+0	1.8E+2	1.7E+3	1.1E+4	1.1E+5	6.6E+5	2.7E+6	7.8E+6
975	1.2E-3	0	3.6E+0	8.1E+1	1.1E+3	7.7E+3	9.8E+4	6.1E+5	2.5E+6	7.1E+6
1025	1.2E-3	0	1.7E+0	4.7E+1	1.2E+3	6.4E+3	8.8E+4	5.7E+5	2.3E+6	6.5E+6

[a]Columns 1 and 2 depict the atmospheric depth x (g cm^{-2}), and the corresponding density ρ (g cm^{-3}), respectively.

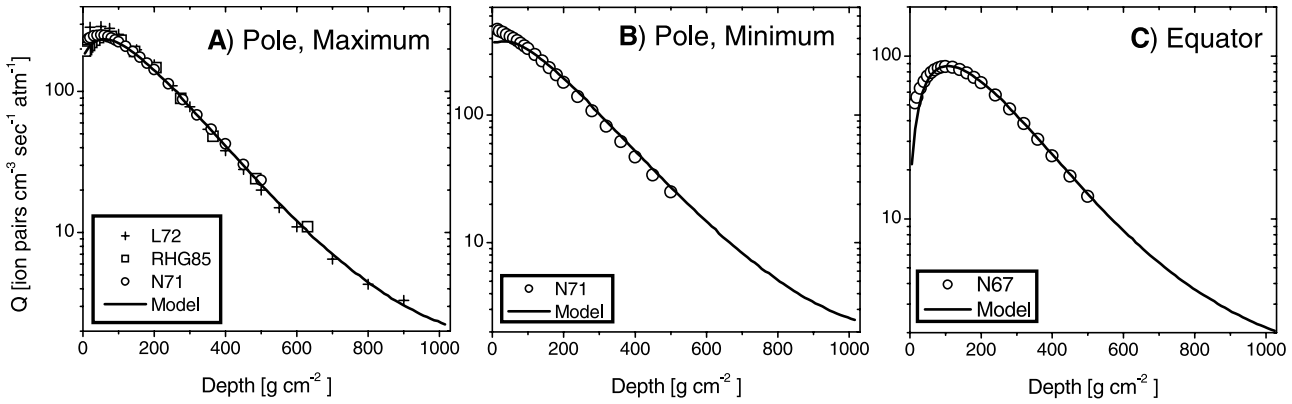

Figure 3. Comparison of the model CRII calculations (solid curve) with direct ionization measurements (symbols). (a) High latitudes during the solar maximum (ϕ = 1000 MV). Symbols correspond to measurements in May 1969 [*Lowder et al.*, 1972] (L72), in May 1979 [*Rosen et al.*, 1985] (RHG85) and in November 1958 [*Neher*, 1971] (N71). (b) Polar regions during the solar minimum (ϕ = 400 MV). Symbols correspond to measurements in July 1965 [*Neher*, 1971] (N71). (c) Equatorial region (P_c = 15 GV) during solar minimum (ϕ = 420 MV). Symbols correspond to a series of balloon-borne measurements in June–July 1965 [*Neher*, 1967] (N67).

slightly lower CRII, in comparison with the measurements; the difference is a few tens of percent. We do not know the exact reason for this discrepancy. It can be, e.g., due to some ionizing agents not related to GCR, due to an effect unaccounted by the model, due to uncertainties of the cosmic ray spectrum, due to a wall effect of the detector, or due to a combination of the effects. Thus the model CRII calculations agree (within 10%) with the actual observations in a whole range of possible parameters, for the lower atmosphere (x > 100 g/cm^2). A discrepancy of 20–50% is found between the model CRII calculations and the measurements in the upper atmosphere, whose nature is not clear.

3. Some Applications

[19] The numerical recipe described above allows one to compute the CRII for a given location (both coordinates and altitude) as a function of the modulation parameter ϕ and the geomagnetic field strength. This provides a useful tool for a quantitative study of the outer space impact on the atmospheric properties, viz., the CRII. Here we illustrate the abilities of the suggested method by means of some practical applications.

[20] First, using a reconstruction of the cosmic ray modulation over the past 54 years [*Usoskin et al.*, 2005], and applying the recipe described in section 2.5, we have computed the CRII since 1951. Figure 4 depicts a time profile of the computed CRII at the atmospheric depth of x = 700 g/cm^2 (at about 3 km altitude), which corresponds to the low clouds, for the polar and equatorial regions. The average ionization rate at the equator is lower, by a factor of 1.6, than that in the polar regions, because of a higher geomagnetic rigidity cutoff. The amplitude of the 11-year cyclic variations of the ionization rate depends on the latitude. Cyclic changes in the low tropospheric CRII are 20–25%, when considered in the polar regions. At the equator, however, they are only about 10%. The difference increases with the altitude, e.g., the amplitude of the solar

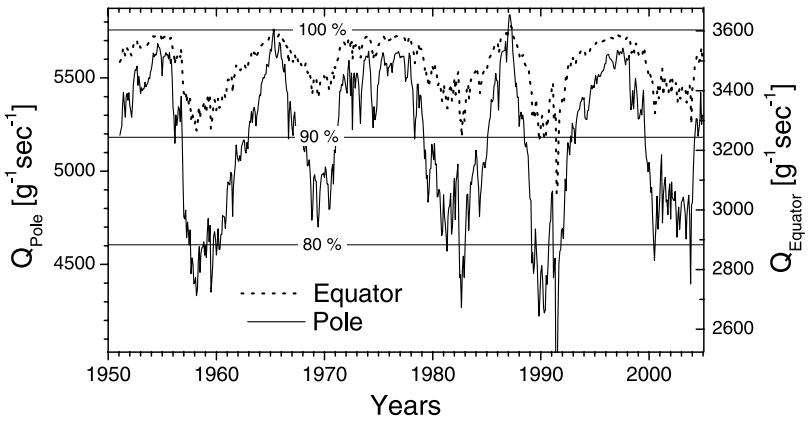

Figure 4. Time profiles of the monthly CRII (ion pairs per gram per second) since 1951 at the atmospheric depth x = 700 g/cm^2 (about 3 km altitude). Solid curve (left axis) corresponds to the polar regions, and dotted curve (right axis) corresponds to the equator. Thin horizontal lines denote the percentage with respect to the values for May 1965 (100%).

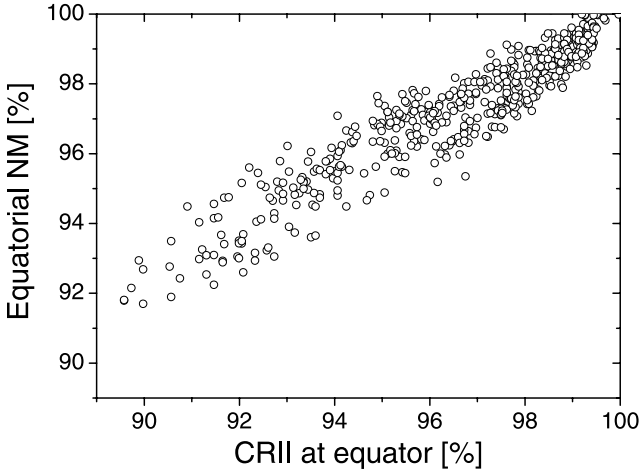

Figure 5. Scatterplot of the monthly count rates (1953–2000) of the equatorial neutron monitor Hunacayo/Haleacala ($P_c \approx 13$ GV) versus the equatorial CRII at the atmospheric depth of $x = 700$ g/cm^2 ($P_c = 15$ GV, see Figure 4). All data have been normalized with respect to the values for May 1965 (100%).

cycle variations for the polar (equatorial) regions at the atmospheric depth $x = 300$ g/cm^2, which roughly corresponds to an upper bound of the troposphere, is 40% (10%).

[21] A ground based neutron monitor is not a one-to-one indicator of the CRII. It detects mostly superthermal neutrons [*Clem and Dorman*, 2000], which correspond to the hadronic component of the atmospheric cascade, while the muon component dominates in the tropospheric CRII, especially at high energies (see Figure 1). Basically, the effective energy of cosmic rays responsible for CRII is different from that measured by the neutron monitors, which somewhat distorts the profile of the cyclic variations. As an illustration, Figure 5 shows the normalized variations of the equatorial neutron monitor count rate and of the equatorial CRII. One can clearly see that the amplitude of the cyclic CRII variations is larger (about 10%) than that in the neutron monitor count rate (about 8%).

[22] It is particularly interesting to evaluate the ionization effect of CR if there was no solar modulation, i.e., $\phi = 0$, which would roughly correspond to the Maunder minimum of solar activity. Figure 6 shows the expected ionization rate at the $x = 700$ g/cm^2 altitude in the polar region, reconstructed for the past 300 years. In order to make this plot, we have used a reconstruction of the modulation potential ϕ by *Usoskin et al.* [2002]. One can see that the CRII, at the depth of 700 g/cm^2 in polar region, was about 40% higher during the Maunder minimum than during the recent solar cycle minima, which is double the variation in the course of the solar cycle (Figure 4). We note that this ratio increases with altitude and geomagnetic latitude [see, e.g., *McCracken et al.*, 2004b].

[23] The maximum effect of CRII is expected in the polar regions [e.g., *Veretenenko and Thejll*, 2004], and detailed study are based on CRII computed separately for different geographical regions [*Pallé et al.*, 2004; *Usoskin et al.*, 2004b]. However, when discussing the possible influence of cosmic ray variations on the global climate, it is still common to use the globally averaged CRII [e.g., *Marsh and Svensmark*, 2003], which can be obtained by integration of equation (6) over the Globe, with the dependence (equation (8)) taken into account. It is not only the solar activity (parameterized by the modulation potential ϕ) that affects the ionization rate, but also the changes of the geomagnetic field, which become crucially important on a long-term scale. Figure 7 shows the globally averaged CRII in the troposphere ($x = 700$ g/cm^2 or about 3 km altitude) as a function of the modulation potential ϕ and the geomagnetic dipole moment with respect to its present day value $M_0 = 7.8\ 10^{22}$ Am^2. We note that $M = 0$ would roughly correspond to a reversal of the geomagnetic field, which occurs regularly on the geological timescales [*Eide and Torsvik*, 1996], while the variations of the dipole moment by a factor of 2 both ways have been observed during the last millennia [*Yang et al.*, 2000; *Korte and Constable*, 2005].

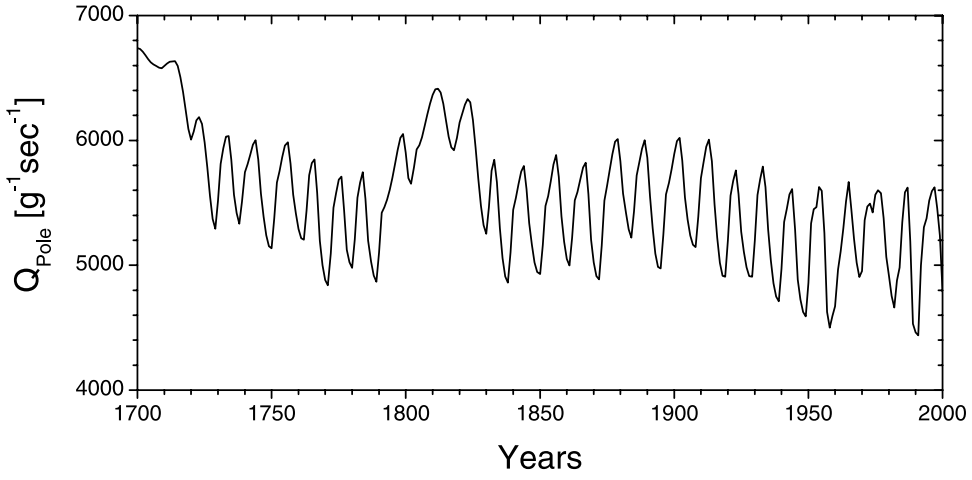

Figure 6. Time profile of the yearly CRII (ion pairs per gram per second), computed after 1700 AD using the cosmic ray flux reconstruction [*Usoskin et al.*, 2002]. The curve corresponds to the CRII at the atmospheric depth $x = 700$ g/cm^2 (about 3 km altitude) in the polar region.

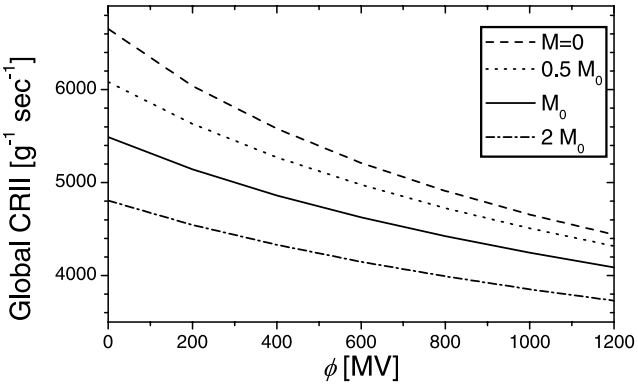

Figure 7. Global cosmic ray induced ionization (ion pairs per gram per second) in the troposphere (at $x = 700$ g/cm^2) as a function of the modulation potential. Different curves correspond to the different strength of the geomagnetic field compared to the present day value M_0, as denoted in the legend.

[24] One can see that the effect of a significant change of the geomagnetic field is at least comparable with the solar cycle variations. Therefore periods of, e.g., the geomagnetic field reversal, when the dipole component nearly vanishes, must result in an enhanced ionization of the atmosphere.

[25] Note that the local interstellar spectrum of GCR J_{LIS} may also vary on the geological timescale, because of, e.g., crossing by the solar system of the galactic spiral arms with a higher density of cosmic rays [*Shaviv*, 2002]. Our method allows evaluating this effect as well provided the corresponding changes of LIS can be estimated.

4. Conclusions

[26] Here we have presented a full numerical model, which computes the cosmic ray induced ionization in the entire atmosphere, from the ground level up to the stratosphere, all over the Globe. The model computations reproduce actual measurements of the atmospheric ionization in the full range of parameters, from equatorial to polar regions and from the solar minimum to solar maximum. A detailed numerical recipe is given in section 2.5 together with the precalculated tabulated ionization yield function (Tables 1 and 2). Using this method, one can easily compute the CRII for any desired location and conditions, instead of using, e.g., a neutron monitor count rate as a proxy. The latter may lead to a distortion of the solar cycle variations in the CRII. The model allows evaluating variations of the CRII caused by the variable solar activity, parameterized by the modulation potential ϕ, and by the slowly changing geomagnetic field. The model allows evaluation of the atmospheric effect of cosmic rays, on different timescales and under different solar/heliospheric conditions. As an example of applications, that can be obtained using this model, we have estimated temporal variations of the CRII during the last 50 years and during the last 300 years, using recent reconstructions of the cosmic ray modulation over these timescales. This approach is applicable also for other planets, after the corresponding simulations of the planet's atmosphere.

[27] Concluding, we have presented a useful and easy-to-use tool to compute the cosmic ray induced ionization in the atmosphere, which can be applied directly to studies of the solar-terrestrial relations and outer space influence on the terrestrial environment.

[28] **Acknowledgments.** We acknowledge the support from the Academy of Finland, the Finnish Academy of Science and Letters (Vilho, Yrjö and Kalle Väisälä Foundation), and the Russian Academy of Sciences (Programme of Fundamental Research 30). We thank the CORSIKA team for continuous update and improvements of the code.

References

Alcaraz, J., et al. (2000), Helium in near Earth orbit, *Phys. Lett. B*, *494*, 193–202.

Aplin, K. L., R. G. Harrison, and A. J. Bennett (2005), Effect of the troposphere on surface neutron counter measurements, *Adv. Space Res.*, *35*, 1484–1491.

Burger, R. A., M. S. Potgieter, and B. Heber (2000), Rigidity dependence of cosmic ray proton latitudinal gradients measured by the Ulysses spacecraft: Implication for the diffusion tensor, *J. Geophys. Res.*, *105*, 27,447–27,455.

Caballero-Lopez, R. A., and H. Moraal (2004), Limitations of the force field equation to describe cosmic ray modulation, *J. Geophys. Res.*, *109*, A01101, doi:10.1029/2003JA010098.

Capdevielle, J. N., et al. (1992), The Karlsruhe Extensive Air Shower Simulation Code CORSIKA, *Rep. KfK 4998*, Kernforsch. Karlsruhe, Karlsruhe, Germany.

Clem, J. M., and L. I. Dorman (2000), Neutron monitor response functions, *Space Sci. Rev.*, *93*, 335–359.

Cooke, D. J. (1983), Geomagnetic-cutoff distribution functions for use in estimating detector response to neutrinos of atmospheric origin, *Phys. Rev. Lett.*, *51*, 320–323.

Desorgher, L., E. O. Flückiger, M. Gurtner, M. R. Moser, and R. Bütikofer (2005), ATMOCOSMICS: A GEANT4 code for computing the interaction of cosmic rays with the Earth's atmosphere, *Int. J. Mod. Phys. A*, *20*, 6802–6804.

Dorman, L. I. (2004), *Cosmic Rays in the Earth's Atmosphere and Underground*, chap. 12, 855 pp., Springer, New York.

Dorman, L. I., and I. V. Dorman (2005), Possible influence of cosmic rays on climate through thunderstorm clouds, *Adv. Space Res.*, *35*, 476–483.

Eide, E. A., and T. H. Torsvik (1996), Paleozoic supercontinental assembly, mantle flushing, and genesis of the Kiaman Superchron, *Earth Planet. Sci. Lett.*, *144*, 389–402.

Elsasser, W., E. P. Ney, and J. R. Winckler (1956), Cosmic-ray intensity and geomagnetism, *Nature*, *178*, 1226–1227.

Fassò, A., A. Ferrari, J. Ranft, and P. R. Sala (2001), FLUKA: Status and prospective of Hadronic applications, in *Proceedings of the Monte Carlo 2000 Conference, Lisbon, 2000*, edited by A. Kling et al., pp. 955–960, Springer, New York.

Fröhlich, C., and J. Lean (2004), Solar radiative output and its variability: Evidence and mechanisms, *Astron. Astrophys. Rev.*, *12*, 273–320.

Gaisser, T. K., and T. Stanev (2004), Cosmic rays, *Phys. Lett. B.*, *592*, 228–234.

Gleeson, L. J., and W. I. Axford (1968), Solar modulation of galactic cosmic rays, *Astrophys. J.*, *154*, 1011–1026.

Gleisner, H., and P. Thejll (2003), Patterns of tropospheric response to solar variability, *Geophys. Res. Lett.*, *30*(13), 1711, doi:10.1029/2003GL017129.

Haigh, J. D. (1994), The role of stratospheric ozone in modulating the solar radiative forcing of climate, *Nature*, *370*, 544–546.

Haigh, J. D. (1996), The impact of solar variability on climate, *Science*, *272*(5264), 981–984.

Haigh, J. D., M. Lockwood, and M. S. Giampapa (2005), *The Sun, Solar Analogs and the Climate*, 424 pp., Springer, New York.

Heck, D., J. Knapp, J. N. Capdevielle, G. Schatz, and T. Thouw (1998), CORSIKA: A Monte Carlo code to simulate extensive air showers, *FZKA 6019*, Forsch. Karlsruhe, Karlsruhe, Germany.

Heck, D., et al. (2003), Influence of low-energy hadronic interaction programs on air shower simulations with CORSIKA, *Proc. Int. Conf. Cosmic Rays 28th*, 279–282.

Keilhauer, B., J. Blümer, R. Engel, H. Klages, and M. Risse (2004), Impact of varying atmospheric profiles on extensive air shower observation: Atmospheric density and primary mass reconstruction, *Astropart. Phys.*, *22*, 249–261.

Korte, M., and C. G. Constable (2005), The geomagnetic dipole moment over the last 7000 years—New results from a global model, *Earth Planet. Sci. Lett.*, *236*, 348–358.

Lowder, W. M., P. D. Raft, and H. L. Beck (1972), Experimental determination of cosmic-ray charged particle intensity profiles in the atmosphere, in Proceedings of the National Symposium on Natural and Manmade Radiation in Space, edited by E. A. Warman, pp. 908–913, NASA, Washington, D. C.

Marsh, N., and H. Svensmark (2003), Solar influence on Earth's climate, *Space Sci. Rev.*, *107*, 317–325.

McCracken, K. G., F. B. McDonald, J. Beer, G. Raisbeck, and F. Yiou (2004a), A phenomenological study of the long-term cosmic ray modulation, 850–1958 AD, *J. Geophys. Res.*, *109*, A12103, doi:10.1029/2004JA010685.

McCracken, K. G., J. Beer, and F. B. McDonald (2004b), Variations in the cosmic radiation, 1890–1986, and the solar and terrestrial applications, *Adv. Space Res.*, *34*, 397–406.

Neher, H. V. (1967), Cosmic ray particles that changed from 1954 to 1958 to 1965, *J. Geophys. Res.*, *72*, 1527–1539.

Neher, H. V. (1971), Cosmic rays at high latitudes and altitudes covering four solar maxima, *J. Geophys. Res.*, *76*, 1637–1651.

Nelson, W. R., H. Hirayama, and D. W. O. Rogers (1985), SLAC-R-265: The EGS4 code system, *Rep. SLAC 265*, Stanford Linear Accel. Cent., Ottawa, Ont., Canada. (Available at http://www.slac.stanford.edu/pubs/slacreports/slac-r-265.html)

Ney, E. P. (1959), Cosmic radiation and the weather, *Nature*, *183*, 451–452.

O'Brien, K. (2005), The theory of cosmic-ray and high-energy solar-particle transport in the atmosphere, in *Proceedings of the 7th International Symposium on the Natural Radiation Environment*, edited by J. P. McLaughlin, S. E. Simopoulos, and F. Steinhusler, pp. 29–44, Elsevier, New York.

Pallé, E., C. J. Butler, and K. O'Brien (2004), The possible connection between ionization in the atmosphere by cosmic rays and low level clouds, *J. Atmos. Sol. Terr. Phys.*, *66*, 1779–1790.

Porter, H. S., C. H. Jackman, and A. E. S. Green (1976), Efficiencies for production of atomic nitrogen and oxygen by relativistic proton impact in air, *J. Chem. Phys.*, *65*, 154–167.

Rosen, J. M., D. J. Hofmann, and W. Gringel (1985), Measurements of ion mobility to 30 km, *J. Geophys. Res.*, *90*(D4), 5876–5884.

Shaviv, N. J. (2002), Cosmic ray diffusion from the galactic spiral arms, iron meteorites, and a possible climatic connection, *Phys. Rev. Lett.*, *89*(5), 051102.

Shaviv, N. J. (2005), On climate response to changes in the cosmic ray flux and radiative budget, *J. Geophys. Res.*, *110*(A8), A08105, doi:10.1029/2004JA010866.

Smart, D. F., M. A. Shea, and E. O. Flückiger (2000), Magnetospheric models and trajectory computations, *Space Sci. Rev.*, *93*, 305–333.

Soon, W. (2005), Variable solar irradiance as a plausible agent for multidecadal variations in the Arctic-wide surface air temperature record of the past 130 years, *Geophys. Res. Lett.*, *32*, L16712, doi:10.1029/2005GL023429.

Tinsley, B. A. (1996), Correlations of atmospheric dynamics with solar wind-induced changes of air-earth current density into cloud tops, *J. Geophys. Res.*, *101*, 29,701–29,714.

Usoskin, I. G., K. Mursula, S. K. Solanki, M. Schüssler, and G. A. Kovaltsov (2002), A physical reconstruction of cosmic ray intensity since 1610, *J. Geophys. Res.*, *107*(A11), 1374, doi:10.1029/2002JA009343.

Usoskin, I. G., O. G. Gladysheva, and G. A. Kovaltsov (2004a), Cosmic ray induced ionization in the atmosphere: Spatial and temporal changes, *J. Atmos. Sol. Terr. Phys.*, *66*(18), 1791–1796.

Usoskin, I. G., N. Marsh, G. A. Kovaltsov, K. Mursula, and O. G. Gladysheva (2004b), Latitudinal dependence of low cloud amount on cosmic ray induced ionization, *Geophys. Res. Lett.*, *31*, L16109, doi:10.1029/2004GL019507.

Usoskin, I. G., K. Alanko-Huotari, G. A. Kovaltsov, and K. Mursula (2005), Heliospheric modulation of cosmic rays: Monthly reconstruction for 1951–2004, *J. Geophys. Res.*, *110*, A12108, doi:10.1029/2005JA011250.

Veretenenko, S., and P. Thejll (2004), Effects of energetic solar proton events on the cyclone development in the North Atlantic, *J. Atmos. Sol. Terr. Phys.*, *66*, 393–405.

Vitt, F. M., and C. H. Jackman (1996), A comparison of sources of odd nitrogen production from 1974 through 1993 in the Earth's middle atmosphere as calculated using a two-dimensional model, *J. Geophys. Res.*, *101*(D3), 6729–6740.

Yang, S., H. Odah, and J. Shaw (2000), Variations in the geomagnetic dipole moment over the last 12000 years, *Geophys. J. Int.*, *140*, 158–162.

G. A. Kovaltsov, Ioffe Physical-Technical Institute, Politekhnicheskaya 26, RU-194021 St. Petersburg, Russia.

I. G. Usoskin, Oulu Unit, Sodankylä Geophysical Observatory, University of Oulu, P.O. Box 3000, FIN-90014 Oulu, Finland. (ilya.usoskin@oulu.fi)